MEASURING LOCAL CRYSTALLIZATION FOULING IN A DOUBLE-PIPE HEAT EXCHANGER

F. Schlüter[1], L. Schnöing[1], H. Zettler[2], W. Augustin[1] and S. Scholl[1]

[1] Technische Universität Braunschweig, Institute for Chemical and Thermal Process Engineering, Langer Kamp 7, 38106 Braunschweig, Germany
E-mail: f.schlueter@tu-braunschweig.de
[2] Heat Transfer Research, Inc. (HTRI), 150 Venture Drive, College Station, TX 77845

ABSTRACT

Although fouling is a problem varying in space and time, sizing and assessment of a process apparatus is almost always based on one single integral fouling resistance value. Furthermore, the integral fluid dynamic behavior, e.g. the development of time-dependent pressure drop in a heat exchanger, can be influenced by local constrictions. While it is generally possible to determine the time dependency of the integral fouling behavior, local differences are not taken into consideration at present. Therefore, this paper introduces a metrological, an incremental and a segmental approach to study the local development of crystallization fouling by $CaSO_4$ in a countercurrent double-pipe heat exchanger. The consecutive approaches allow for thermal, volumetric, gravimetric and optical fouling investigations, aiming to examine the axial distribution of deposit as well as local differences in the deposit morphology. All methods provided congruent results and local fouling could be described properly. An almost clean surface at the colder end of the heat exchanger and an exponential increase of deposit thickness was observed towards the hot end. Hence, the section near to the hot water inlet turned out to be a key area with regards to increasing fouling mass and structural changes of the layer.

INTRODUCTION

Fouling describes unwanted deposits formed on heat transfer surfaces and is a major challenge for industry. Therefore, fouling has been a subject to scientific investigations for decades (Müller-Steinhagen, 2011). The literature provides many works on the investigation of time-dependent integral behavior of crystallization fouling with respect to various scientific issues (Bohnet and Augustin, 1993; Krause, 1993; Augustin and Bohnet, 1995; Helalizadeh et al., 2000; Müller-Steinhagen et al., 2000; Zettler et al., 2005; Al-Janabi et al., 2009; Pääkkönen et al., 2012), but only a few have been published on the local distribution of fouling.

Fahiminia et al. (2007) equipped an electrically heated tube section length of 770 mm with ten thermocouples to investigate local initial fouling rates of $CaSO_4$. The tube was subsequently cut into segments 20 mm long to allow for optical investigation and examining the deposit coverage by means of mass, layer thickness and morphology. An increasing amount of non-homogeneous fouling deposit was found as the wall temperatures increased.

Local crystallization fouling of $CaSO_4$ was investigated in double-pipe heat exchangers of 2000 mm length heated by water in countercurrent flow (Albert et al., 2011). A borescope was used for visual examination of deposits at several axial positions along the inner heat exchanger tubes. This revealed an increasing surface area covered with deposit towards the hot heat exchanger end. Following a fouling experiment, photographs of tube inlet and outlet were analyzed resulting in the assumption of an idealized linear increase of the fouling distribution between those axial positions. Furthermore, a volumetric method by means of a water displacement test was applied to identify the flow cross section constricted by deposit at the tube outlet.

Goedecke et al. (2016) equipped the heat exchanger test sections of the same test rig with five thermocouples at different axial positions, evenly spaced along the tube length. The local fouling curves obtained confirmed the increase in the amount of deposit in the direction of hot wall temperatures, see Fig. 1.

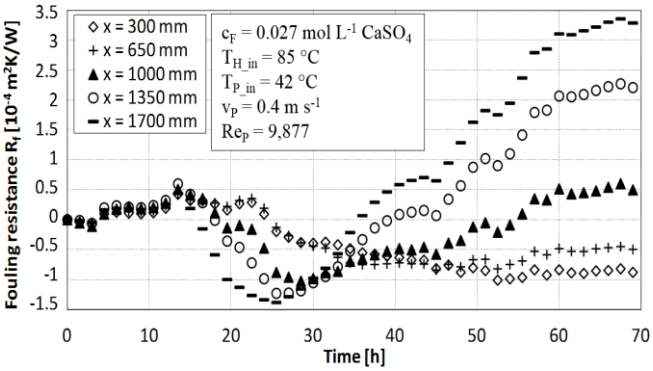

Fig. 1 Local fouling resistances over time for a stainless steel heat exchanger tube of 2000 mm length (adapted from Goedecke et al., 2016); x is the distance from inlet.

Building on these promising insights, the present work continues the investigations of local fouling behavior. Therefore, methods already applied in the past are combined and partly extended by precise local examinations.

ISBN: 978-0-9984188-0-3; Published online www.heatexchanger-fouling.com

Furthermore, the applicability of a novel approach, using a fiber optic system for estimating local thermal fouling resistances is demonstrated. This comprehensive approach aspires to gain knowledge about the axial distribution of fouling layers developing in a countercurrent heat exchanger as well as the effects on the overall heat transfer.

EXPERIMENTAL PROCEDURE

Fouling experiments

Experiments with an aqueous $CaSO_4$ solution were carried out in the fouling test rig shown in Fig. 2.

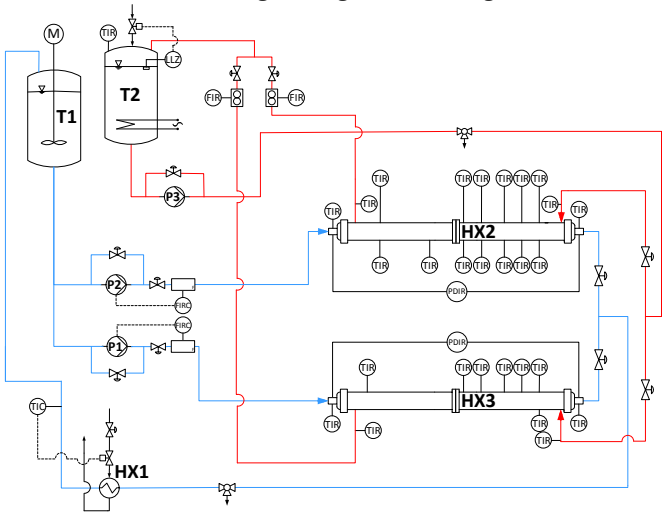

Fig. 2 Fouling test rig equipped with two double-pipe heat exchangers, a heating circuit and a product circuit.

The core components of the experimental setup are two stainless steel double-pipe heat exchangers (HX2, HX3) of identical design. Two fluid streams pass through the test sections in counterflow with hot water on shell side and the product solution (deionized water with 0.027 mol L^{-1} $CaSO_4$) on the tube side. The product is provided in tank T1 with a volume of 50 L and separated in two mass flows downstream. Centrifugal pumps P1 and P2 (KSB, Movitec VF 2/6 and VF 2/4) pump the solution with a constant inlet temperature of 42 °C through the inner pipes (20 x 2 x 2000 mm) of the heat exchangers. The two flows join and are cooled by plate frame heat exchanger HX1 (GEA Ecoflex, Ecoflex VT04) to 42 °C using water from an on-site cooling water circle before the flow enters tank T1. Flow is measured with inductive flow meters (Krohne, OPTIFLUX 1100 C) and controlled by throttle valves and additional bypasses. Fouling experiments were conducted with flow velocities of 1.0 and 1.5 m s^{-1} (Re_p = 25,500 and 38,200). Temperatures were measured with type K thermocouples at the inlets and outlets of both test sections and at several local measuring points along the wall of the inner tube. The pressure drop over heat exchanger length was measured by differential pressure sensors (Honeywell, FDW2JG). All materials in contact with the product fluid are made of glass or stainless steel.

Tank T2 is equipped with two electrical heaters (ISA Heinrich Industrietechnik, IST/9 and IST/4) with a total controllable heating power of 13 kW and provides 150 L of hot water at 80 °C. The centrifugal pump P3 (KSB, Movitec VF 2/6) circulates the water with v_s = 0.25 m s^{-1} (Re_s = 20,700) through the test rig.

The plant was cleaned prior to every fouling test with deionized water at different flow velocities, followed by a cleaning solution with 2 wt% acetic acid for at least 12 hours. Several consecutive water cleaning treatments were performed until the water's electrical conductivity matched the conductivity of pure deionized water.

Metrological approach

Integral and local fouling resistances were extracted as indicators for the fouling situation. The integral thermal fouling resistance of both heat exchangers is based on temperature measurements of the in- and outlet streams and quantifies the change in the overall heat transfer resistance at soiled $\left(\frac{1}{k_f}\right)$ and clean $\left(\frac{1}{k_0}\right)$ state according to Eq. (1).

$$R_{f,int} = \frac{1}{k_f(t)} - \frac{1}{k_0} \quad (1)$$

In order to investigate the fouling situation locally by determining local fouling resistances, two different techniques are applied in the present work. One of the test sections (HX2) is equipped with seven thermocouples located along the annular clearance between the inner and outer tube to measure shell side temperatures, see Fig. 3. Furthermore, six thermocouples are located in bores of 1 mm depth in the inner tube wall and fixed by soldering joints to measure wall temperatures. The nonuniform distribution of thermocouples was selected to give better resolution of temperatures in the downstream section of the tube where the highest amount of fouling deposit is expected due to the countercurrent flow arrangement of the heat exchanger.

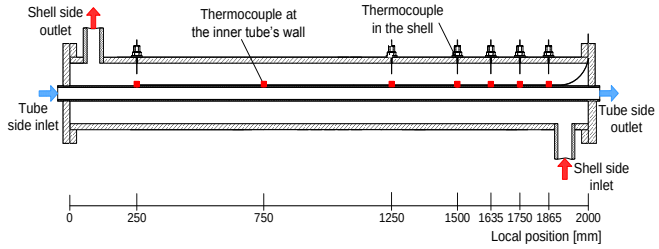

Fig. 3 Double-pipe heat exchanger test section 2 (HX2) equipped with thermocouples at several axial positions on the shell side and in the tube wall for local temperature measurements.

For quantifying thermal fouling resistances locally, Eq. (1) is written as:

$$R_{f,loc} = \frac{1}{k_f(t,z)} - \frac{1}{k_0(z)} \quad (2)$$

The local overall heat transfer coefficients are calculated based on the temperature difference between the inner wall surface of the test tube and the bulk of the product stream. Furthermore, the heat flux at the inner wall surface is used:

$$k_f(t,z) = \frac{\dot{q}_i(t,z)}{T_{w,i}(t,z) - T_b(t,z)} \quad (3)$$

ISBN: 978-0-9984188-0-3; Published online www.heatexchanger-fouling.com

Local temperatures at the inner wall surface ($T_{w,i}$) and within the bulk (T_b) need to be calculated since the heat exchangers are not designed for measuring these directly. Local bulk temperatures are obtained by linear regression between inlet and outlet temperatures. Local wall temperatures are calculated with measured wall temperatures $T_{w,M}$, the heat flux at the measuring point $\dot{q}_M$ and the overall heat transfer coefficient due to thermal resistance from measuring point to the inner wall surface $k_{0,Mi}$ (VDI-Wärmeatlas, 2013):

$$T_{w,i}(t,z) = T_{w,M}(t,z) - k_{0,Mi} \cdot \dot{q}_M(t,z) \qquad (4)$$

The second heat exchanger (HX3) is equipped with a fiber optic temperature measurement sensor. This technique allows temperatures to be determined with an axial resolution below 10 mm. In the present work a measuring interval of 20 mm was applied to allow for a higher local resolution of the temperature profile compared to HX2.

The fiber-based measurement system features an active monitoring unit which is connected to the passive sensor fiber (Luna, ODiSI A50). The monitoring unit transmits light into the fiber from a broadband source. Characteristics of the light traveling within the fiber are modified as a function of temperature and strain. These changes are detected in the backscattered light which is later collected by the monitoring unit, analyzed and then converted into strain and temperature data.

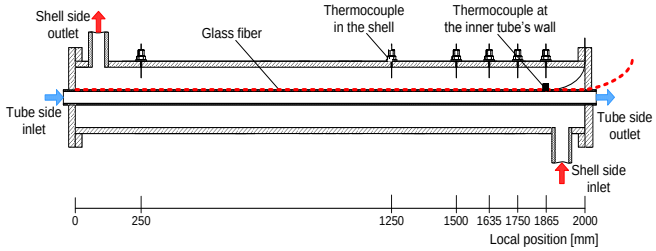

Fig. 4 Double-pipe heat exchanger test section 3 (HX3) equipped with thermocouples in the shell side and glass fiber sensor in the tube wall for local temperature measurements.

Fig. 4 shows a sketch of the double-pipe exchanger (HX3) equipped with the fiber sensor. Local thermocouples in the annular gap determine the temperature profile of the shell side flow. A thermocouple in the tube wall next to the fiber sensor at z = 1865 mm serves as reference temperature measuring point. The glass fiber, 0.3 mm in diameter, is surrounded by a spring steel capillary of 0.8 mm in diameter and is fixed in a groove of 1 mm depth within the tube wall by a number of soldering joints. Fig. 5 demonstrates the positions of sensor and thermocouples within the double-pipe. Since the force of the turbulent hot water inlet stream on the shell side may cause interference with the sensitive measurement signal, the sensor and the corresponding thermocouple are installed at the opposite side.

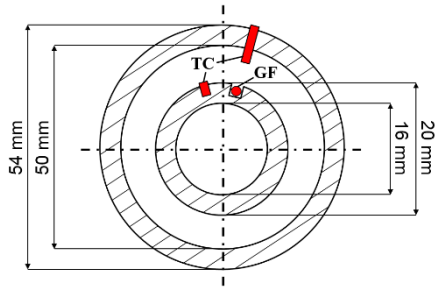

Fig. 5 Illustration of the location of thermocouples (TC) and glass fiber sensor (GF) in the double-pipe walls.

Incremental approach

In order to allow local investigations the inner tube of HX2 is replaced by a new stainless steel tube without thermocouples. This tube can be dismounted after a fouling experiment to investigate the axial distribution of deposit incrementally regarding its volume. Assuming identical fouling progress in test sections HX2 and HX3, the glass fiber sensor in HX3 provides the associated temperature profile during a test run.

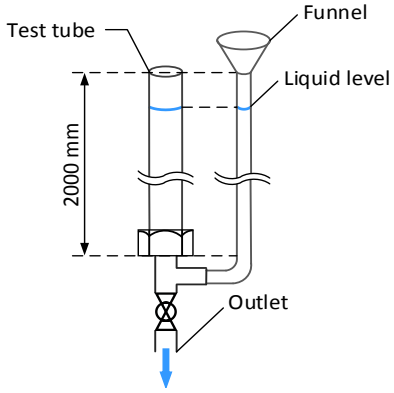

Fig. 6 Sketch of the procedure used to determine axial distribution of volume of fouling deposit.

The basic concept of the incremental approach is to determine the local volume of fouling deposits inside the tube by using the principle of communicating tubes, see Fig. 6. A test tube and a translucent tube are connected with a T-piece. A funnel on top of the translucent tube is used as water inlet and a ball valve serves as water outlet. Initially, a clean tube is mounted and filled incrementally with defined volumes of deionized water. The liquid level rises equally in both tubes and is noted for each volume added to the tubes until the entire height of 2000 mm is reached. Subsequently, the clean tube is replaced by a fouled tube and the procedure is repeated. The tube from a fouling experiment is dried by storing in ambient air for several days before usage. Afterwards, liquid levels are noted while filling and compared to those of the clean tube. This allows the local volume of deposit to be calculated.

Segmental approach

Subsequently to the volumetric investigation, mass and morphology of deposits as well as the thickness of the fouling layer are examined locally by a segmental approach. The fouled test tube is cut into eight segments of 250 mm length using a tube cutter. Cutting the tube has to be done very

cautiously to minimize damage to the deposit. A sketch of the segmentation is given in Fig. 7. As illustrated, most deposit is expected in the segment between z = 1750 and 2000 mm.

After optical inspection, photographs of cross sections of every segment are taken with a digital camera. The image analysis software ImageJ is used to determine the thickness of fouling layer at each cross section. This reveals the local constriction of the area free for flow along the tube length.

Additional micrographs of local deposits are taken with a scanning electron microscope (Zeiss, EVO LS 25) for assessing differences of the layer morphology depending on their axial position.

Besides visual investigations, the segments are used for a gravimetrical analysis as supplementary information to the local distribution of deposits. After weighing of segments, they are cleaned of all deposits by applying an acetic acid solution and weighed again.

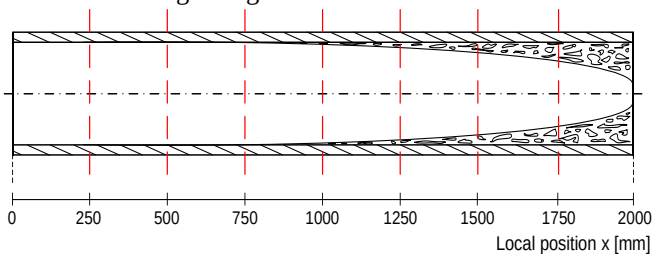

Fig. 7 Sketch of the fouled test tube showing cuts into segments of 250 mm length to investigate the deposit.

RESULTS

Integral and local fouling resistance

Thermal fouling investigations were carried out with the test rig equipped with heat exchanger tubes as illustrated in Fig. 3 and 4. The resulting integral and local fouling resistances for both test sections are presented for a fouling experiment with a flow velocity of 1.0 m s^{-1} and an experimental time of about 5 days.

Fig. 8 shows time-dependent integral fouling curves for HX2 and HX3. Generally, both curves follow the same trends despite of separating slightly at t = 2 d. After negative values during the roughness controlled period, an approximately linear increase can be seen for both plots. A minor sequence of leveling and sharper rises is owed to the periodic addition of salts (Na_2SO_4 and $Ca(NO_3)_2{\cdot}4H_2O$) into the product stream in order to restore the product concentration to 0.027 mol L^{-1} $CaSO_4$. The current salt concentration and the necessary amount of salts were determined by titration. Fouling formation accelerated as soon as the oversaturation of the solution was increased again.

Inspection of the integral fouling curves reveals no significant difference between the tube fouling behaviors. Therefore, both heat exchangers show a comparable decrease in their thermal efficiency due to fouling.

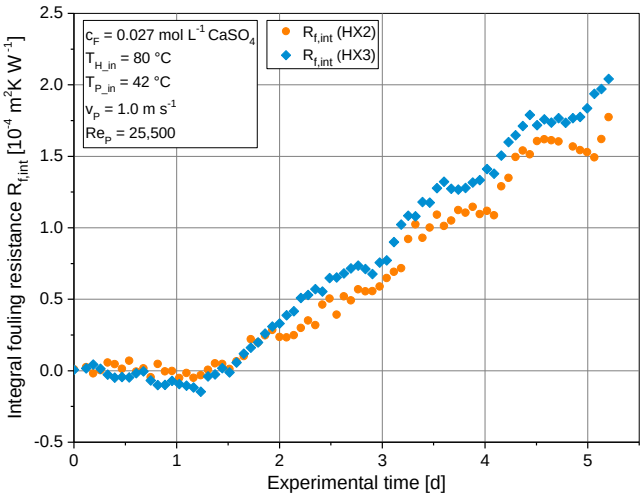

Fig. 8 Integral thermal fouling resistances over time for both test sections on the basis of measured inlet and outlet temperatures.

Local temperature measurements reveal distinct differences between the axial positions, see Fig. 9. Four of seven local fouling curves are presented since practically no decrease in heat transfer was detected up to the axial position z = 1500 mm. The first significantly increasing fouling curve was found at z = 1635 mm. All plots show an initiation and a roughness controlled period whose duration relates to the distance between the axial position of the measuring points and the hot water inlet. Following those periods, crystal growth starts and results in increasing local fouling resistances until the end of the experiment.

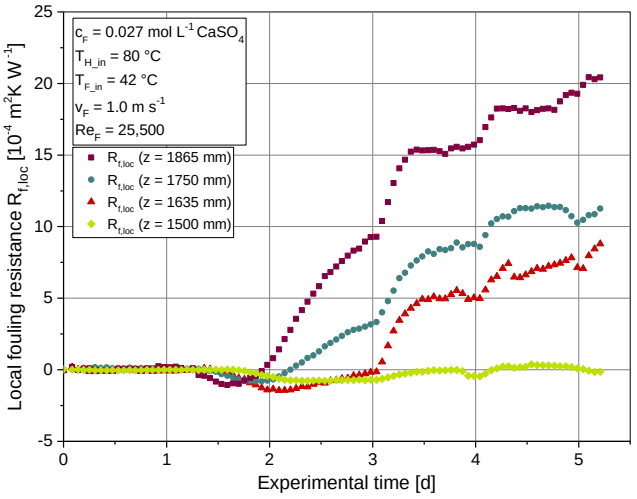

Fig. 9 Local fouling resistances over time on the basis of wall temperatures measured locally with thermocouples at four axial positions on HX2.

Results of the thermal investigation by evaluating the glass fiber sensor measurements are presented in Fig. 10. The axial resolution was initially set to a measurement interval of 20 mm. Selected fouling curves are shown to demonstrate the capabilities of the technique and for comparison with Fig. 9. The experimental conditions were identical to those of HX2. Again, all curves clearly relate to the distance between the location of the measuring point and the hot water inlet. Approaching the hot water inlet increases the fouling rate and

ISBN: 978-0-9984188-0-3; Published online www.heatexchanger-fouling.com

the final fouling resistance. In contrast to Fig. 9, an increase in fouling resistance is evident already at axial position z = 1380 mm. At z = 1240 mm only deposits enhancing the flow turbulence exist, resulting in negative fouling resistance. The curve does not leave the roughness controlled period during the entire experimental time. The plot of z = 1960 mm shows the most significant enhancement of heat transfer after around one day. Therefore, a fast development of the surface roughness can be assumed at that location. This goes along with the highest surface and bulk temperatures at this axial position. Contrary to Fig. 9, the periodic addition of salts did not result in a similarly sharp stepwise increase, e.g. the course of z = 1860 mm levels off at 3.5 days and does not increase sharply after addition of salts at t = 4 d.

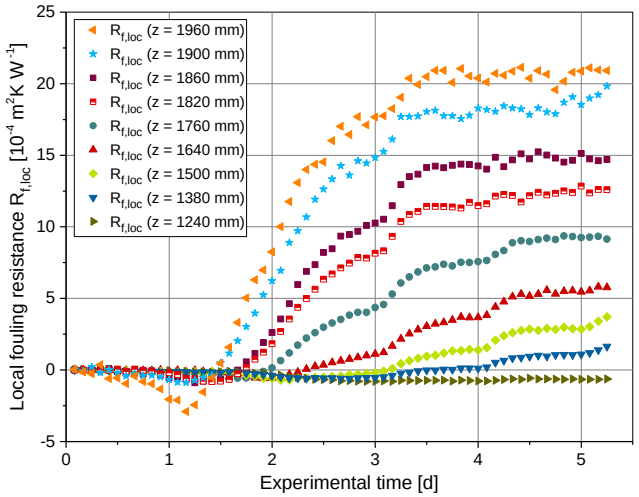

Fig. 10 Local fouling resistances over time on the basis of wall temperatures measured locally with the glass fiber sensor at several axial positions of HX3 (operating conditions were identical to those of HX2, Fig. 9).

In conclusion, local fouling resistances are reasonable if looking at the results based on both temperature measurement techniques separately. The high local fouling values also seem to be reasonable after comparing with the fouling layers typically build up within the experiments (see Fig. 13). Although both heat exchangers have identical operating conditions, fouling behavior cannot be exactly the same, even if integral fouling resistances are similar. Local variations of fouling build-up lead to uncertainties concerning fouling detection by applying thermocouples since each thermocouple (diameter 1 mm) measures temperatures at one defined axial position. In contrast, the glass fiber sensor allows consistent measurements (averaged over 10 mm) with a higher local resolution which can be helpful to reveal unexpected local differences. Therefore, results provided by the glass fiber sensor measurements are considered to be more precise. Slight differences in wall temperatures ($T_{w,M}$) measured by the thermocouples and glass fiber sensor at the start of an experiment when no deposit is present indicate a systematic difference in temperatures at the inner wall surface ($T_{w,i}$), see Eq. (4). This is attributed to the different techniques of fixing local thermocouples and fiber sensor in the tube wall.

According to Eq. (5), the calculated wall temperatures directly influence the calculated local heat flux at the inner wall surface ($\dot{q}_i$) especially since measured shell side temperatures (T_s) and the overall heat transfer coefficient from shell side to inner wall surface ($k_{0,si}$) are nearly identical for both test sections.

$$\dot{q}_i(t,z) = k_{0,si} \cdot \left(T_s(t,z) - T_{w,i}(t,z)\right) \qquad (5)$$

Different local heat fluxes result in deviations regarding local overall heat transfer coefficients and local fouling resistances. In combination with the differences obtained from the two measurement techniques this explains the different fouling values at comparable axial positions of both heat exchangers (see Fig. 9 and 10). In order to overcome the issue of differing fouling resistances, there is a need for optimizing the numerical evaluation by taking the deviations between temperatures measured with thermocouples and fiber sensor into account.

All following results refer to two different fouling experiments and were obtained by applying the incremental and segmental approaches to demonstrate further possibilities of investigating the fouling behavior locally. Two new tubes without thermocouples or fiber sensor were used and results of fouling experiments with a fluid velocity of 1.0 and 1.5 m s^{-1} are reported and compared for each investigation method.

Distribution of local volume and local mass of deposits

For investigating volume and mass of deposit locally the incremental and segmental approaches were applied after fouling experiments with fluid velocities of 1.0 and 1.5 m s^{-1} and experimental times of 9 and 17 days respectively. The test runs are used to verify the applicability of the local investigation methods. Due to the different experimental times, a comparison of both data sets is not prioritized in this paper.

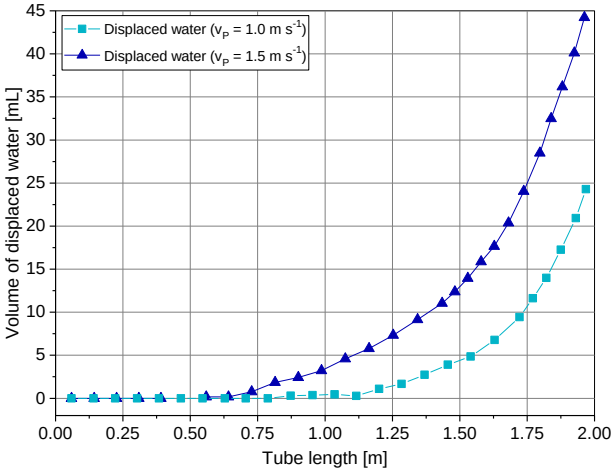

Fig. 11 Accumulated volume of displaced water over time indicating the local distribution of volume occupied by deposits inside the fouled tube.

Fig. 11 shows the accumulated volumetric occupation of the inner tube volume by fouling deposits. In case of the test with

v_P = 1.0 m s^{-1} no displaced water is detected up to a tube length of 1000 mm. Subsequently, the curve starts to rise very slightly and then increases exponentially until the full length of 2000 mm is reached with an accumulated volume of 25 mL.

The experiment with a flow velocity of 1.5 m s^{-1} shows a similar length-dependent curve. However, there are distinct differences regarding the amount of displaced water. The course of the curve starts to rise exponentially at around 600 mm and ends with a maximum volume of displaced water of almost 45 mL, which is nearly twice the volume of the experiment with 1.0 m s^{-1}.

In conclusion, both plots indicate an exponential increase of deposit volume towards the heat exchanger hot end. Though, a larger water volume is displaced by fouling at v_P = 1.5 m s^{-1}. Most likely this finding is caused by three factors: (i) a thicker layer was formed at various axial positions causing less free cross sectional area, (ii) fouling is formed along a longer section of the tube (iii) a more compact fouling layer with less cavity for water. The first two aspects are related to the longer experimental time of the test run, the third to the higher flow velocity. For a direct comparability test runs of different flow velocities have to be carried out with identical experimental time. In that case a higher flow velocity would result in less deposits.

The determination of local fouling mass by using the heat exchanger tubes of both test runs was performed as a part of the segmental approach. Figure 12 shows increasing mass of deposits along the tube length, with the major increment from segment 7 to 8. A total mass of 62 g was obtained for the experiment with v = 1.0 m s^{-1}. Most of the deposit (26 g) was found in segment 8. Only marginal amounts of deposit (below 1 g) were detected in the first two segments. For the longer experiment, at v_P = 1.5 m s^{-1}, a significantly higher amount of deposit accumulated in total (99 g) and the local mass in segment 8 (around 43.5 g) was noticeably larger.

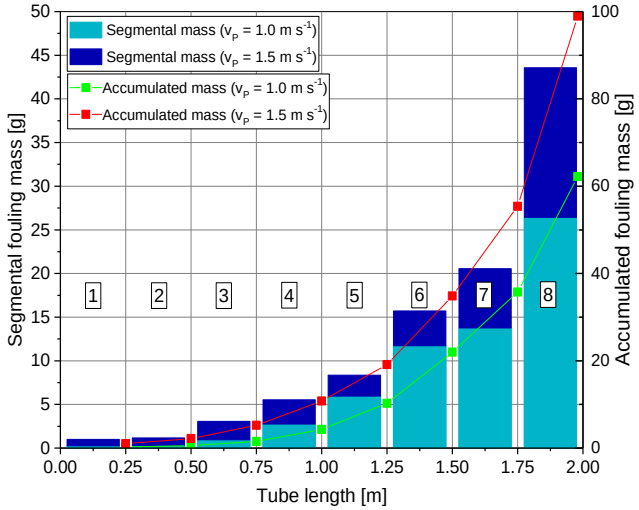

Fig. 12 Distribution (accumulated and segmental) of local mass of deposits obtained by weighing tube segments of 250 mm length.

These results are consistent with the volumetric analysis. The trend of increasing fouling build-up in direction of the hot water inlet and therefore with increasing tube length is confirmed. Furthermore, the consistently higher fouling mass also approves that the experiment with higher flow velocity and experimental time results in a more compact and/or a thicker fouling layer inside the tube. In addition, the accumulated masses of the first three to four tube segments expose the volumetric analysis as a not sufficiently sensitive measurement technique for detecting the first 5 g of deposits, since no displaced water volume was detected at these positions (cp. Fig. 11).

Local thickness and morphology of fouling deposits

All tube segment cross sections were photographed for further inspection of fouling layers. Selected axial positions are compared in Fig. 13 and 14 to demonstrate the length-dependent development of the fouling layer as well as the corresponding constriction. The difference between the fouling build-up at local positions 1750 and 2000 mm is evident. Furthermore, the formed layer does not completely cover the tube surface at z = 500 mm. Fig. 14 additionally shows that the fouling layer of the test run with 1.5 m s^{-1} ended being more compact compared with the other experiment.

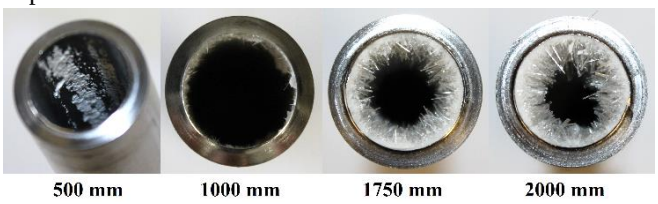

Fig. 13 Photographs of cross-sections at different axial positions of the cut fouling test tube for a fluid velocity of 1.0 m s^{-1} after 9 days.

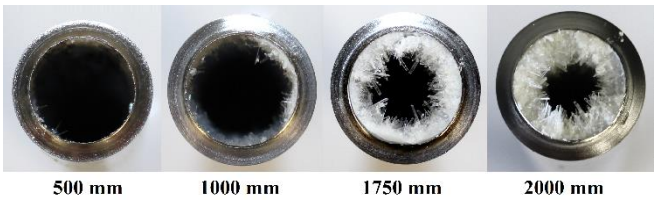

Fig. 14 Photographs of cross-sections at different axial positions of the cut fouling test tube for a fluid velocity of 1.5 m s^{-1} after 17 days.

Figure 15 shows examples of the layer thickness at different locations identified using image analysis software.

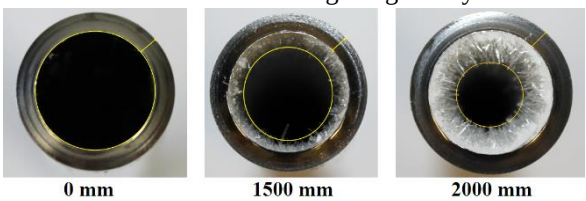

Fig. 15 Procedure of the image evaluation demonstrated with cross-sections at different axial positions after a fouling experiment with a fluid velocity of 1.0 m s^{-1}.

The thickness measurement addresses the compact base layer as well as crystal needles and does not distinguish

between these two structures. According to Eq. (6), the layer thickness $x_{f,picture}$ is calculated as the difference between diameter of flow cross-section without (d_0) and with fouling ($d_{f,picture}$).

$$x_{f,picture}(z) = \frac{d_0 - d_{f,picture}(z)}{2} \qquad (6)$$

The evaluation works best in case of flow cross sections uniformly constricted by deposit as they are in Fig. 15. A near-circular geometry of the cross section without fouling is applied and its equivalent tube diameter $d_{f,picture}$ is estimated.

Results of cross-sections at axial positions 1000, 1250, 1500, 1750 and 2000 mm from both fouling experiments are compared in Fig. 16. No fouling was found below z = 1000 mm and 750 mm respectively. Layer thicknesses obtained from the test run with v_P = 1.5 m s^{-1} are consistently higher than those of the experiment with lower flow velocity, which agrees with the other methods. The major increase of fouling layer thickness was found between cross sections at 1500 to 1750 mm in both experiments. Subsequently, high local flow velocities based on local constrictions are present. The effective wall shear stress will be larger and is expected to suppress layer growth to some extent. Thus, the proportion of compact base layer increases which accounts for the larger amount of deposit (cp. Fig. 11, 12, 13 and 14).

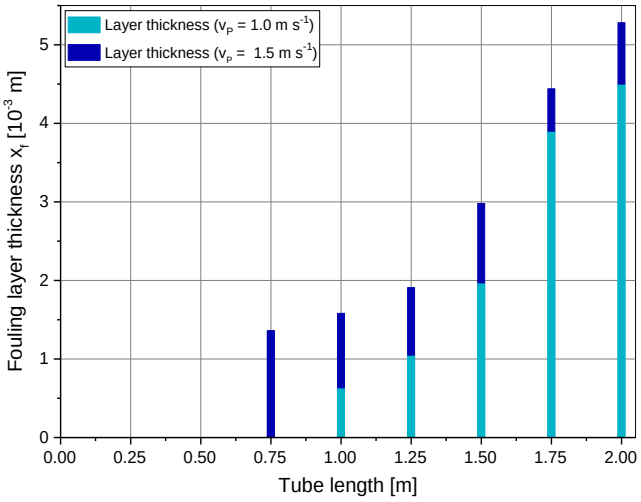

Fig. 16 Local thickness of fouling layers as result of the image analysis of cross sections after cutting the test tubes into segments.

In addition to the photographs, SEM micrographs of deposits obtained from the fouling experiment with 1.0 m s^{-1} are shown in Fig. 17. Randomly orientated needle-like crystals grow thicker and longer at larger z. Furthermore, the mesh of needles is packed more densely and the base layer gets less visible towards the hot water inlet. The difference in layer morphology between z = 1250 and 2000 mm is notable and supports the importance of the downstream section of the tube regarding local fouling investigations.

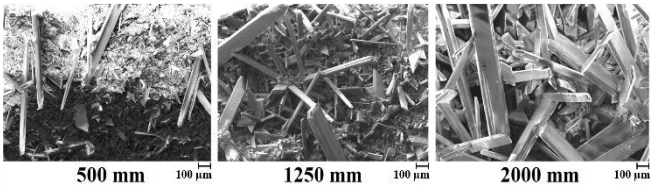

Fig. 17 SEM micrographs of fouling deposits at different axial positions (all 50x magnification) after the experiment with a fluid velocity of 1.0 m s^{-1}.

CONCLUSIONS

Three different approaches (metrological, incremental and segmental) were used to assess integral vs. local fouling progress during crystallization fouling of $CaSO_4$. As part of these approaches several measuring techniques were applied for investigating crystallization fouling locally in a double-pipe heat exchanger to reveal the distribution of deposit along the apparatus.

From thermal investigations, the axial distribution of local deposits and the decrease of overall heat transfer were obtained. The measurements obtained by the glass fiber sensor were considered to be more precise because of the technique's independence of axial variations regarding fouling build-up and its higher local resolution.

Further local fouling investigations (volumetric, gravimetric and optical) underlined findings from the thermal analysis. The downstream section between z = 1750 and 2000 mm turned out to be a key area with regards to increasing fouling mass and volume, as well as structural changes within the layer. High effective shear stresses resulting from constrictions of free flow cross section in this area influenced the morphology of the fouling layers.

The surface was free of deposit at the colder end of the heat exchanger and an exponential increase of deposition when approaching the hot water inlet was observed. The approaches presented provide reasonable and congruent findings. Applying the different methods will be continued with the common objective of correlating local temperature measurements with the corresponding fouling layer thickness and morphology.

NOMENCLATURE

c_F	concentration fouling fluid, mol L^{-1}
d	tube diameter, m
k	overall heat transfer coefficient, W m^{-2}K^{-1}
q	heat flux, W m^{-2}
Re	Reynolds number, -
R_f	thermal fouling resistance, m^{2}K W^{-1}
t	experimental time, d
T	temperature, °C
v	flow velocity, m s^{-1}
x_f	fouling layer thickness, m
z	axial position, m

Subscripts

0	without fouling
b	bulk
f	with fouling

ISBN: 978-0-9984188-0-3; Published online www.heatexchanger-fouling.com

H_in	hot water inlet
i	inner
int	integral
loc	local
M	measuring point
Mi	from measuring point to inner wall surface
P	product stream
P_in	product stream inlet
picture	based on photograph
s	shell side
si	from shell side to inner wall surface
w	wall

Acronyms

$Ca(NO_3)_2{\cdot}4H_2O$	calcium nitrate tetrahydrate
$CaSO_4$	calcium sulphate
GF	glass fiber sensor
HX2	double-pipe heat exchanger test section 2
HX3	double-pipe heat exchanger test section 3
Na_2SO_4	sodium sulphate
SEM	Scanning Electron Microscope
TC	thermocouple

ACKNOWLEDGMENT

Special thanks go to the technicians of the Institute for Chemical and Thermal Process Engineering, namely Karl Karrenführer, Jörg Leppelt, Sven Lorenzen and Nils Bergmann, for the construction of the heat exchanger test sections and the great support in case of any issue regarding the test rig.

REFERENCES

Albert, F., Augustin, W., and Scholl, S., 2011, Roughness and constriction effects in crystallization fouling, *Chem. Eng. Sci.*, Vol. 66 (3), pp. 499-509.

Al-Janabi, A, Malayeri, M.R., and Müller-Steinhagen, H, 2009, Experimental investigation of crystallization fouling on grooved stainless steel surfaces during convective heat transfer, *Heat Transfer Eng.*, Vol 30 (10-11), pp. 832-839.

Augustin, W., and Bohnet, M, 1995, Influence of the ratio of free hydrogen ions on crystallization fouling, *Chem. Eng. Process.*, Vol. 34 (2), pp. 79-85.

Bohnet, M., and Augustin, W, 1993, Effect of surface structure and pH-value on fouling behaviour of heat exchangers, in J. S. Lee et al.: Transport Phenomena in Thermal Engineering, Begell House, New York, pp. 884-889.

Fahiminia, F., Watkinson, A.P., and Epstein, N., 2007, Early events in the precipitation fouling of calcium sulphate dihydrate under sensible heating conditions, *Can. J. Chem. Eng.*, Vol. 85 (5), pp. 679–691.

Goedecke, R., Drögemüller, P., Augustin, W., and Scholl, S., 2016, Experiments on integral and local crystallization fouling resistances in a double-pipe heat exchanger with wire matrix inserts, *Heat Transfer Eng.*, Vol. 37 (1), pp. 24-31.

Helalizadeh, H., Müller-Steinhagen, H., and Jamialahmadi, M., 2000, Mixed salt crystallization fouling, *Chem. Eng. Process*, Vol. 39 (1), pp. 29-43.

Krause, S., 1993, Fouling of heat transfer surfaces by crystallization and sedimentation, *Int. Chem. Eng.*, Vol. 33 (3), pp. 335-401.

Müller-Steinhagen, H., 2011, Heat Transfer Fouling: 50 years after the Kern and Seaton model, *Heat Transfer Eng.*, Vol 32 (1), pp. 1-13.

Müller-Steinhagen, H., Zhao, Q., Helali-Zadeh, A., and Ren, X.-G., 2000, The effect of surface properties on $CaSO_4$ scale formation during convective heat transfer and subcooled flow boiling, *Can. J. Chem. Eng.*, Vol. 78 (1), pp. 12-20.

Pääkkönen, T.M., Riihimäki, M., Simonson, C.J., Muurinen, E., and Keiski, R.L., 2012, Crystallization fouling of $CaCO_3$ – Analysis of experimental thermal resistance and its uncertainty, *Int. J. Heat Mass Transfer*, Vol. 55 (23-24), pp. 6927-6937.

VDI-Wärmeatlas, 2013, Springer Verlag Berlin Heidelberg, Chapter B2.

Zettler, H.U., Weiss, M., Zhao, Q., and Müller-Steinhagen, H., 2005, Influence of surface properties and characteristics on fouling in plate heat exchangers, *Heat Transfer Eng.*, Vol. 26 (2), pp. 3-17.